IEEE Access
Multidisciplinary | Rapid Review | Open Access Journal

Received April 20, 2021, accepted April 27, 2021, date of publication May 3, 2021, date of current version May 13, 2021.

Digital Object Identifier 10.1109/ACCESS.2021.3076990

Nonlinear Fractional Active Disturbance Rejection Speed Control for Stabilization of Hydraulic Turbine Regulating Systems With Mechanical Delay

BO AI, TING LIU, ZHE ZHANG, AND BIN WANG, (Member, IEEE)
College of Water Resources and Architectural Engineering, Northwest A&F University, Xianyang 712100, China
Key Laboratory of Agricultural Soil and Water Engineering in Arid and Semiarid Areas, Ministry of Education, Northwest A&F University, Xianyang 712100, China

Corresponding author: Bin Wang (binwang@nwsuaf.edu.cn)

This work was supported in part by the Scientific Research Foundation of the Young Scholar Project of Cyrus Tang Foundation, in part by the Shaanxi Province Key Research and Development Plan under Grant 2021NY-181 and Grant 2017NY-112, and in part by the National Natural Science Foundation of China under Grant 51909222 and Grant 51809218.

ABSTRACT An improved fractional-order nonlinear active disturbance rejection speed control (FO-NADRC) method is proposed for hydraulic turbine regulating systems (HTRSs) with a mechanical delay. First, the mathematical model of an HTRS with a mechanical time delay is established. Based on the principle of coordinate transformation, the state space equation of an HTRS with a time delay is transformed into the controllable normative mathematical model. Second, a new nonlinear function is proposed for the extended state observer ESO) that improves the observation accuracy and suppresses the high-frequency oscillation of the HTRS. Third, a new fractional-order state error feedback law (FO-SEFL) is proposed by introducing double adjustable parameters. Fourth, according to the improved ESO and the FO-SEFL, a novel FO-NADRC is designed for the HTRS. Furthermore, the Popov-Lyapunov robust stability analysis method is used to analyze the stability of the hydraulic turbine regulating control systems with mechanical delay. Finally, numerical simulation experiments demonstrate the effectiveness and superiority of the proposed control scheme.

INDEX TERMS Hydraulic turbine regulating system, time delay, fractional-order nonlinear active disturbance rejection control, extended state observer, the Popov-Lyapunov robust stability.

NOMENCLATURE

HYDRAULIC TURBINE REGULATING SYSTEM (HTRS)

μ	*Generator rotor angle deviation*
ω	*Rotational speed relative deviation of the generator*
m_t	*Hydraulic turbine output incremental torque deviation*
y	*Incremental deviation of the guide vane opening*
ω_0	*Rated rotation speed of generator (rad/s)*
T_{ab}	*Inertia time constants (s)*
D	*Damping coefficient of the generator*
T_w	*Water inertia time constant (s)*
T_y	*Reaction time constant of the relay (s)*
E'_q	*Transient electromotive force of the q-axis*
$x'_{d\sum}$	*Transient reactance of the d-axis*
$x_{q\sum}$	*Synchronous reactance of the q-axis*
V_s	*Infinite system bus voltage of the power system*
e	*Transfer coefficient*
e_{qh}	*Transfer coefficient of turbine flow on the head*
e_y	*Transfer coefficient of turbine torque on the main servomotor stroke*

TRACKING DIFFERENTIATOR DESIGN (TD)

fhan	*Nonlinear synthesis function*
h_0	*Filter factor*
r_0	*Velocity factor*
h	*Sampling period*

NONLINEAR EXTENDED STATE OBSERVER (ESO)

α	*Nonlinear factor*

The associate editor coordinating the review of this manuscript and approving it for publication was Lei Chen.

σ *Nonlinear factor*
δ *Linear interval width*
β_{01} *Observer gain coefficient*
β_{02} *Observer gain coefficient*
β_{03} *Observer gain coefficient*
β_{04} *Observer gain coefficient*

STATE ERROR FEEDBACK LAW (SEFL)

u *Control input*
K_p *Control law proportional gain coefficient*
K_i *Control law integral gain coefficient*
K_d *Control law differential gain coefficient*
λ *Adjustable parameter*
γ *Adjustable parameter*
b_0 *Compensation factor*

I. INTRODUCTION

With the substantial increase in energy consumption, the global energy supply and demand is generally tight. There are growing calls for greater use of renewable energy [1]. Renewable energy use is the key condition for changing the current unreasonable energy consumption structure. China could achieve sustainable social and economic development by improving the status of renewable energy in its energy structure. In recent years, China's hydropower industry has entered a stage of rapid growth with the development of hydropower resources [2]. In 2019, China's total installed hydropower capacity increased by 4.17 GW. China's hydropower capacity is expected to reach 380 GW in 2020 [3]. Therefore, the safety and stabilization of the hydropower system are facing more complex challenges. The HTRSs are the hubs of the hydropower stations for converting the potential energy of water into electric energy, and their stability plays a vital role in maintaining the safe operation of the power grid. Therefore, it is very important to design a reliable controller for the stable operation of the HTRSs [4].

The HTRS is a concentration of hydraulic machinery, a mechanical system, electrical load, and a control system for the integration of the system. In the actual operation of hydropower stations, the various components of the HTRS interact with and influence each other through coupling [5]. As an extension of integer order, fractional calculus has advantages in nonlinear modeling and nonlinear control [6]–[8]. Therefore, the design of an effective fractional-order controller can improve the precision control performance of an HTRS system [9].

In the process of production operation, the operating conditions of an HTRS are constantly changing. Under the action of the traditional proportional-integral-derivative (PID) controller [10], it is very difficult to ensure that all working conditions of an HTRS have good control quality [11], [12]. Furthermore, the HTRS has mechanical delays when the system signals are collected and processed, and the hydraulic servo system adjusts the guide vane opening [13]–[15], which makes stabilization control more difficult.

With deeper research on ''classical control theory'' and ''modern control theory,'' Han proposed active disturbance rejection control (ADRC) to compensate for the defects of PID control [16]. ADRC can suppress the disturbance by estimating and eliminating it in real time. The disturbance compensation device (DCD) can estimate and compensate for various uncertainties within the system and cross-coupled disturbances between channels [17]. In recent years, with deeper research, ADRC has been successfully applied to the control of various uncertain industrial processes involving the flight system [18], trajectory tracking system [19], motor system [20], power system [21], etc. The literature [19] analyzed the stability and robustness of the NADRC for the three-dimensional trajectory tracking control system with mismatched uncertainties. The phenomenon of delays has a great influence on uncertain nonlinear systems. The research on time-delay compensator has also developed rapidly [22]–[25], such as the output feedback compensator [22], and the predictor compensator [25]. The existing research primarily focuses on linear ADRC, such as the stability analysis of linear ADRC [26], analysis of ADRC for systems with uncertainty and delay [27], and exponential stability analysis of a closed-loop system [28]. However, few theoretical studies are on nonlinear ADRC systems. In Ref. [29], the convergence and stability problems of ADRC based on nonlinear extended state observer have been solved. In Ref. [30], ADRC is applied to the uncertain nonlinear system with external bounded random perturbations. Despite NADRC studies, it is a common problem that high-frequency buffeting occurs to a certain extent after the system reaches a steady state [31]. In addition, ADRC is primarily used for typical single-input single-output (SISO) systems or the standard ADRC model at present, and the multidimensional nonlinear system is rarely studied. No report on the ADRC of nonlinear hydraulic turbine regulating systems is available. Can FO-NADRC be used for stability regulation of nonlinear time-delay HTRS? If possible, how can the nonlinear HTRS model be matched with ADRC? How can the mechanical delay in the HTRS be solved? How can the phenomenon of high-frequency chattering in the system be solved? Therefore, what are the specific NADRC forms and stability analysis derivations that are applied to nonlinear HTRS? Because the above problems have not been reported, research in this field should be meaningful and challenging.

Inspired by the above analysis and discussion, the main contributions of this article are as follows. First, based on the principle of coordinate transformation, the nonlinear HTRS model is transformed into a matching ADRC model. Second, a new nonlinear function is proposed to improve the classical ESO to avoid the high-frequency oscillation caused by the symbolic function in the traditional ADRC. Third, two adjustable parameters are introduced to design an FO-SEFL to improve the adaptive capacity of the controller to the historical dependence of the hydraulic servo system. Fourth, a new FO-ADRC is designed for the hydraulic turbine regulating systems with mechanical delay. In addition, the stabilization

of the NADRC is analyzed using the Popov-Lyapunov robust stability analysis method. Finally, the effectiveness and superiority of the proposed scheme are verified via numerical simulation.

The remainder of this study is organized as follows: In Section 2, a nonlinear HTRS with time delay is introduced. The nonlinear fractional-order ADRC controller is presented and makes a rigorous theoretical analysis in Section 3. Numerical simulations are shown in Section 4. In Section 4, numerical simulation is performed for different working conditions. Section 5 concludes this paper.

II. MATHEMATICAL MODEL OF THE NONLINEAR HTRS

The hydraulic turbine regulating system is presented as in reference [5]:

$$\begin{cases} \dot{\mu} = \omega_0 \omega \\ \dot{\omega} = \dfrac{1}{T_{ab}} \left[m_t - D\omega - \dfrac{E'_q V_S}{x'_{d\Sigma}} \sin\mu - \dfrac{V_s^2}{2} \dfrac{x'_{d\Sigma} - x_{q\Sigma}}{x'_{d\Sigma} x_{q\Sigma}} \sin\ 2\mu \right] \\ \dot{m}_t = \dfrac{1}{e_{qh} T_w} \left[-m_t + e_y y - \dfrac{e e_y T_w}{T_y} (u - y) \right] \\ \dot{y} = \dfrac{1}{T_y} (u - y) \end{cases} \tag{1}$$

The parameters of HTRS (1) are provided in Table 1 [32]. u is the control input, which needs to be designed later.

Given that the hydraulic servo system has a strong historical dependence and mechanical inertia, a hydraulic servo system with a time delay is introduced [33]:

$$y = y(t) = \begin{cases} y(t-\tau), & t \in [\tau, +\infty] \\ y_0, & t \in [0, \tau] \end{cases} \tag{2}$$

where τ is the time delay and $\tau > 0$; y_0 is the initial value for the state variable.

By combining (1) and (2), a time-delay HTRS is presented as

$$\begin{cases} \dot{\mu}(t) = \omega_0 \omega \\ \dot{\omega}(t) = \dfrac{1}{T_{ab}} \left[m_t - D\omega - \dfrac{E'_q V_S}{x'_{d\Sigma}} \sin\mu(t) \right. \\ \left. - \dfrac{V_s^2}{2} \dfrac{x'_{d\Sigma} - x_{q\Sigma}}{x'_{d\Sigma} x_{q\Sigma}} \sin\ 2\mu(t) \right] \\ \dot{m}_t(t) = \dfrac{1}{e_{qh} T_w} \left[-m_t + e_y y(t-\tau) \right. \\ \left. - \dfrac{e e_y T_w}{T_y} (u - y(t-\tau)) \right] \\ \dot{y}(t) = \dfrac{1}{T_y} \left[u - y\,(t-\tau) \right] \end{cases} \tag{3}$$

III. CONTROLER DESIGN

A. MODEL TRANSFORMATION

The ADRC is primarily composed of a tracking differentiator (TD), extended state observer (ESO), and linear state error feedback law (SEFL) [34]. The structure of the ADRC is shown in Figure 1.

TABLE 1. Parameters of the HTRS.

Symbol	Value	Symbol	Value
ω_0	314 rad/s	$x'_{d\Sigma}$	1.25
T_{ab}	19.0 s	$x_{q\Sigma}$	1.474
D	2.0	V_s	1.0
E'_q	1.35	e	0.7
T_w	0.8 s	e_{qh}	0.5
T_y	0.1 s	e_y	1.0

TD can reasonably extract continuous signals and differential signals to solve the problem of signal discontinuity. ESO expands the disturbance function that affects the output of the controlled object into a new state variable, which is used to solve the problem of disturbance observation in active disturbance rejection technology. SEFL combines the three signals of error, error differentiation and error integration to form a combined control rate to realize signal feedback and compensation.

In Figure 1, v is the speed input signal, v_1 and v_2 and are the approximate input signal and differential signal extracted by TD, respectively. e_1 and e_2 are error signals. z_1, z_2 and z_3 are status observation signals. u_0 is the nonlinear feedback control, and x is the turbine speed relative deviation.

For convenience, HTRS (3) is represented as

$$\begin{cases} \dot{\mu}(t) = f_1(\mu, \omega, m_t, y, t) \\ \dot{\omega}(t) = f_2(\mu, \omega, m_t, y, t) \\ \dot{m}_t(t) = f_3(\mu, \omega, m_t, y, t) \\ \dot{y}(t) = f_4(\mu, \omega, m_t, y, t) \\ y_o(t) = \omega(t) \end{cases} \tag{4}$$

where

$$\begin{cases} f_1(\mu, \omega, m_t, y, t) = \omega_0 \omega \\ f_2(\mu, \omega, m_t, y, t) = \dfrac{1}{T_{ab}} \left[m_t - D\omega - \dfrac{E'_q V_S}{x'_{d\Sigma}} \sin\mu(t) \right. \\ \left. - \dfrac{V_s^2}{2} \dfrac{x'_{d\Sigma} - x_{q\Sigma}}{x'_{d\Sigma} x_{q\Sigma}} \sin\ 2\mu(t) \right] \\ f_3(\mu, \omega, m_t, y, t) = \dfrac{1}{e_{qh} T_w} \left[-m_t + e_y y(t-\tau) \right. \\ \left. - \dfrac{e e_y T_w}{T_y} (u - y(t-\tau)) \right] \\ f_4(\mu, \omega, m_t, y, t) = \dfrac{1}{T_y} \left[u - y\,(t-\tau) \right], \end{cases}$$

and y_o is the system output.

Because $f_1(\mu, \omega, m_t, y, t)$, $f_2(\mu, \omega, m_t, y, t)$, $f_3(\mu, \omega, m_t, y, t)$ and $f_4(\mu, \omega, m_t, y, t)$ are continuously differentiable, the system can be observed. There is

$$g(\mu, \omega, m_t, y, t) = \dot{f}_2(\mu, \omega, m_t, y, t)$$

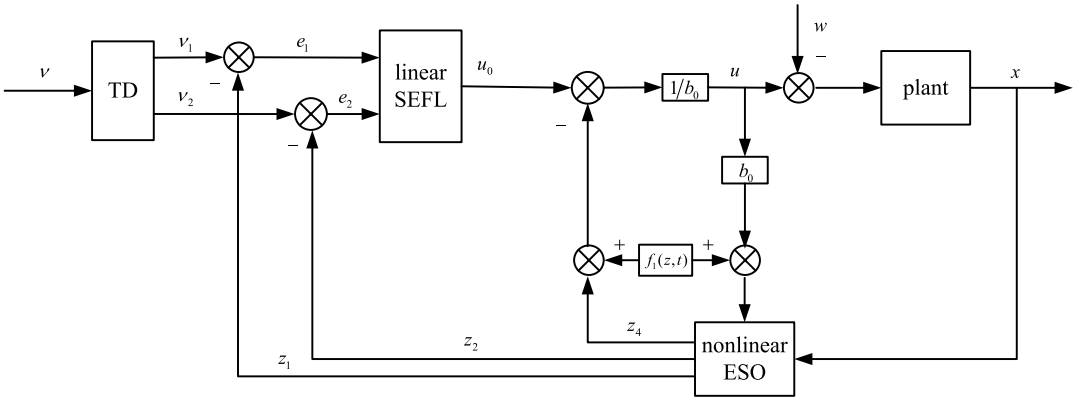

FIGURE 1. NADRC structure block diagram.

$$= \frac{\delta f_2}{\delta \mu} f_1 + \frac{\delta f_2}{\delta \omega} f_2 + \frac{\delta f_2}{\delta m_t} f_3 + \frac{\delta f_2}{\delta y} f_4 \quad (5)$$

Then,

$$\begin{aligned}
&g(\mu, \omega, m_t, y, t) \\
&= \ddot{\omega} \\
&= \frac{1}{T_{ab}} \left(\dot{m}_t - D\dot{\omega} - \frac{E'_q V_s \cos\mu(t)}{x'_{d\sum}} \dot{\mu}(t) \right. \\
&\quad \left. - \frac{V_s^2 (x'_{d\sum} - x_{q\sum}) \cos 2\mu(t)}{x'_{d\sum} x_{q\sum}} \dot{\mu}(t) \right) \\
&= \frac{1}{T_{ab}} \left\{ \frac{1}{e_{qh} T_w} \left[-m_t + e_y y(t-\tau) \right. \right. \\
&\quad \left. - \frac{e e_y T_w}{T_s} (u(t) - y(t-\tau)) \right] \\
&\quad - \frac{D}{T_{ab}} \left(m_t - D\omega - \frac{E'_q V}{x'_{d\sum}} \sin\mu(t) \right. \\
&\quad \left. - \frac{V_s^2}{2} \frac{x'_{d\sum} - x_{q\sum}}{x'_{d\sum} x_{q\sum}} \sin 2\mu(t) \right) \\
&\quad \left. - \left(\frac{E'_q V_s \cos\mu(t)}{x'_{d\sum}} + \frac{V_s^2 (x'_{d\sum} - x_{q\sum}) \cos 2\mu(t)}{x'_{d\sum} x_{q\sum}} \right) \omega_0 \omega \right\} \\
&= \frac{1}{T_{ab}} \left\{ \left(\frac{D^2}{T_{ab}} - \frac{E'_q V_s \omega_0 \cos\mu(t)}{x'_{d\sum}} \right. \right. \\
&\quad \left. - \frac{V_s^2 (x'_{d\sum} - x_{q\sum}) \omega_0 \cos 2\mu(t)}{x'_{d\sum} x_{q\sum}} \right) \omega \\
&\quad - \left(\frac{D}{T_{ab}} + \frac{1}{e_{qh} T_w} \right) m_t + \left(\frac{e e_y}{T_s e_{qh}} + \frac{e_y}{e_{qh} T_w} \right) y(t-\tau) \\
&\quad \left. + \frac{D}{T_{ab}} \left(\frac{E'_q V_s}{x'_{d\sum}} \sin\mu(t) + \frac{V_s^2}{2} \frac{x'_{d\sum} - x_{q\sum}}{x'_{d\sum} x_{q\sum}} \sin 2\mu(t) \right) \right\} \\
&\quad - \frac{e e_y}{e_{qh} T_{ab} T_s} u(t) \\
&= F(x,t) - \frac{e e_y}{e_{qh} T_{ab} T_s} u(t) \qquad (6)
\end{aligned}$$

where

$$\begin{aligned}
&F(x,t) \\
&= \frac{1}{T_{ab}} \left\{ \left(\frac{D^2}{T_{ab}} - \frac{E'_q V_s \omega_0 \cos\mu(t)}{x'_{d\sum}} \right. \right. \\
&\quad \left. - \frac{V_s^2 (x'_{d\sum} - x_{q\sum}) \omega_0 \cos 2\mu(t)}{x'_{d\sum} x_{q\sum}} \right) \omega \\
&\quad - \left(\frac{D}{T_{ab}} + \frac{1}{e_{qh} T_w} \right) m_t + \left(\frac{e e_y}{T_s e_{qh}} + \frac{e_y}{e_{qh} T_w} \right) y(t-\tau) \\
&\quad \left. + \frac{D}{T_{ab}} \left(\frac{E'_q V_s}{x'_{d\sum}} \sin\mu(t) + \frac{V_s^2}{2} \frac{x'_{d\sum} - x_{q\sum}}{x'_{d\sum} x_{q\sum}} \sin 2\mu(t) \right) \right\}
\end{aligned} \quad (7)$$

Let

$$\begin{cases} x_1(t) = \omega(t) \\ x_2(t) = \dot{\omega}(t) \\ x_3(t) = g(\mu, \omega, m_t, y, t) \end{cases} \quad (8)$$

According to Equations (4) and (6), one has

$$\begin{cases} \dot{x}_1(t) = x_2(t) \\ \dot{x}_2(t) = x_3(t) \\ \dot{x}_3(t) = f(x,t) + bu \\ y_o(t) = x_1(t) \end{cases} \quad (9)$$

Rewrite (9) as

$$\begin{cases} \dot{x}_1(t) = x_2(t) \\ \dot{x}_2(t) = x_3(t) \\ \dot{x}_3(t) = f_1(x,t) + g(x,u,t) + bu \\ y_o(t) = x_1(t) \end{cases} \quad (10)$$

where $f_1(x,t) = a_3 x_1(t) + a_2 x_2(t) + a_1 x_3(t)$, $g(x,u,t) = f(x,t) + (b - b_0)u$, and $f_1(x,t)$ represents the modeled linear dynamics; $g(x,u,t)$ is treated as the total disturbances that represent the combined effects of the internal nonlinear and unmodeled dynamics and external disturbances. x_1 is the state

variable of the system. The time-delay term of the system is considered the unknown disturbance of the system.

B. CONTROLLER DESIGN

When the classical ADRC is used to address the system nonlinearity, the system will undergo adverse phenomena, such as overshoot and high-frequency buffeting. Based on the NADRC designed in [35] and considering the complexity of the nonlinear HTRS, the improved ADRC can be designed from the following perspectives. First, the proposed nonlinear function is introduced into the classical ESO, and a new observer is designed. Second, two adjustable parameters are introduced to design a new, adjustable SEFL. Finally, the improved ESO and SEFL are combined to design a nonlinear FO-NADRC.

1) TRACKING DIFFERENTIATOR DESIGN

The discrete form of the TD is expressed as

$$\begin{cases} x_1(k+1) = x_1(k) + hx_2(k) \\ x_2(k+1) = x_2(k) - r_0u(k), |u(k)| \le r_0 \end{cases} \tag{11}$$

where x_1 and x_2 are the system state, h_0 is the filter factor, and h is the sampling period.

A nonlinear synthesis function is as

$$\begin{cases} d = r_0h_0^2, \\ a_0 = h_0x_2, \\ y = x_1 + a_0 \\ a_1 = \sqrt{d(d+8|y|)} \\ a_2 = a_0 + sign(y)(a_1 - d)/2 \\ s_y = (sign(y+d) - sign(y-d))/2 \\ a = (a_0 + y - a_2)s_y + a_2 \\ s_a = (sign(a+d) - sign(a-d))/2 \\ fhan = -r\,[a/d - sign(a)]\,s_a - r_0sign(a) \end{cases} \tag{12}$$

The TD is designed as [36]

$$\begin{cases} fh = fhan(v_1(t) - v(t), v_2, r_0, h_0) \\ v_1(t+1) = v_1(t) + hv_2(t) \\ v_2(t+1) = v_2(t) + hfh \end{cases} \tag{13}$$

2) NONLINEAR EXTENDED STATE OBSERVER

According to "the small error in the large gain, large error of the small gain" engineering characteristics of thoughts, this paper proposes a nonlinear smooth function $g(x, \sigma)$. In the design of the extended state observer, the function $fal(x, \alpha, \delta)$ [35] is replaced by $g(x, \sigma)$.

The proposed nonlinear smooth function $g(x, \sigma)$ is defined as follows:

$$\varphi(x) = \begin{cases} g(x,\sigma) = \dfrac{x}{\sigma^2}\exp(-x^2/2\sigma^2) \\ f(x,\alpha,\delta) = \begin{cases} \dfrac{x}{\delta^{(1-\alpha)}}, |x| \le \delta \\ sign(x)\,|x|^{\alpha}, |x| > \delta \end{cases} \end{cases} \tag{14}$$

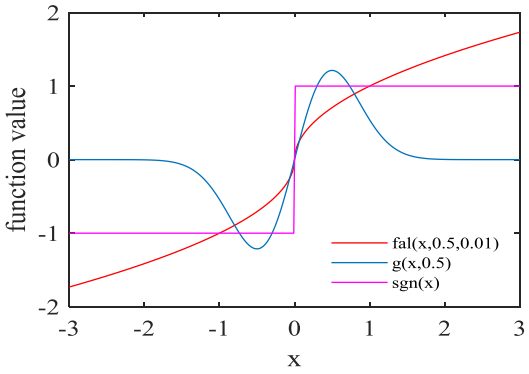

FIGURE 2. Function curves of $sgn(x)$, $fal(x, \alpha, \delta)$ and $g(x, \sigma)$.

The figure shows that $g(x, \sigma)$ has the following characteristics:

(1) $g(0, \sigma) = 0; g(\pm\infty, \sigma) = 0$;

(2) When $x = -\sigma$, $g(x, \sigma)$ obtains the minimum of $g(-\sigma, \sigma) = -\frac{1}{\sigma\sqrt{e}}$; when $x = \sigma$, $g(x, \sigma)$ obtains the maximum of $g(\sigma, \sigma) = \frac{1}{\sigma\sqrt{e}}$; e is the base of the natural logarithm.

As shown in Figure 2, compared with the functions $sgn(x)$ and $fal(x, \alpha, \delta)$, function $g(x, \sigma)$ completely avoids the high-frequency oscillation caused by the symbolic function. In addition, function $g(x, \sigma)$ has an immune function to the large error. Therefore, as long as the immune factor σ is properly set, $g(x, \sigma)$ is beneficial for improving the estimation performance of the ESO.

Let the observation error be $e = z_1 - y$. The nonlinear smooth function $g(x, \sigma)$ is substituted for the nonlinear power function $fal(x, \alpha, \delta)$ to obtain a new extended state observer.

$$\begin{cases} e = z_1(t) - y_o(t) \\ \dot{z}_1(t) = z_2(t) - \beta_{01}g_1(e, \sigma_1) \\ \dot{z}_2(t) = z_3(t) - \beta_{02}g_1(e, \sigma_2) \\ \dot{z}_3(t) = z_4(t) - \beta_{03}g_1(e, \sigma_3) + f_1(z, t) + b_0u \\ \dot{z}_4(t) = -\beta_{04}g_1(e, \sigma_4) \end{cases} \tag{15}$$

where $f_1(z, t) = a_3z_1(t) + a_2z_2(t) + a_1z_3(t)$, z_1 is the state tracking of the actual speed x_1, z_2 is the state tracking of the differential speed signal x_2, and z_4 is the estimated value of the unknown disturbance $g(x, u, t)$ of the system.

3) FRACTIONAL-ORDER STATE ERROR FEEDBACK LAW

The error signals generated by the TD and ESO are used as input signals to form a feedback law. Using the error signal e_1 and error differential signal e_2, the error integral signal e_0 can be generated to realize linear feedback. The traditional controller is designed as follows:

$$u_0(t) = \sum_{n=1}^{2} k_ne_n(t) = K_p(v_1 - z_1) + K_d(v_2 - z_2) \tag{16}$$

The fractional-order PID expands the stability domain of the control system and provides stronger robustness of the

time-varying parameters in the process of modeling and control [37]. The controller performance becomes more flexible by adding adjustable parameters λ and γ. The fractional-order controller has better nonlinear characteristics in the HTRS [38].

The fractional Riemann-Liouville integral is defined as

$$ {}_aD_t^r f(t) = \frac{1}{\Gamma(n-r)} \frac{d^n}{dt^n} \int_a^t \frac{f(\tau)}{(t-\tau)^{r-n-1}} d\tau \tag{17} $$

where $\Gamma(\cdot)$ is the Gamma function and $n-1 < r < n$.

The fractional-order SEFL is defined from the perspective of transfer function as follows:

$$ G(s) = \frac{U(s)}{E(s)} = K_p' + K_i' s^{-\lambda} + K_d' s^{\gamma}, \quad (\lambda, \gamma > 0) \tag{18} $$

From the perspective of time domains, the output of the fractional-order SEFL is designed as [39]:

$$ u_0(t) = K_p' e_1(t) + K_i' D^{-\lambda} e_1(t) + K_d' D^{\gamma} e_2(t) \tag{19} $$

The original target is reduced to a series standard control problem of the integrator, and the controller is designed as

$$ u = \frac{u_0 - f_1(z,t) - z_4}{b_0} \tag{20} $$

C. ROBUST STABILITY ANALYSIS

1) SYSTEM TRANSFORMATION ASSUMPTION

Assumption: The input v is zero, and all the outputs $v_i (i = 1, 2)$ are zero for TD (13).

Substitute Equations (16) and (20) into Equation (10), and let $X = [x_1, x_2, x_3]^T$ and $Z = [z_1, z_2, z_3]^T$.

$$ \begin{cases} \dot{X} = A_{11}X + A_{12}Z + A_{13}(z_4 - g(x,u,t)) \\ y_o = x_1 \end{cases} \tag{21} $$

where

$$ A_{11} = \begin{bmatrix} 0 & 1 & 0 \\ 0 & 0 & 1 \\ a_3 & a_2 & a_1 \end{bmatrix}, \quad A_{12} = \begin{bmatrix} 0 & 0 & 0 \\ 0 & 0 & 0 \\ -k_1 - a_3 & -k_2 - a_2 & -a_1 \end{bmatrix}, $$

$$ A_{13} = \begin{bmatrix} 0 & 0 & -1 \end{bmatrix}^T \in R^n, \quad v_i (i = 1, 2). $$

Substituting Equations (16) and (20) into Equation (15) obtains

$$ \begin{cases} \dot{Z} = A_{21}Z + A_{22}u' \\ z_4 = \beta_{04}u' \\ u' = -\phi(e) \end{cases} \tag{22} $$

where

$$ A_{21} = \begin{bmatrix} 0 & 1 & 0 \\ 0 & 0 & 1 \\ -k_1 & -k_2 & 0 \end{bmatrix}, \quad A_{22} = \begin{bmatrix} \beta_{01} & \beta_{02} & \beta_{03} \end{bmatrix}^T. $$

Combining (21) and (22) obtains

$$ \begin{cases} \dot{X} = A_{11}X + A_{12}Z + A_{13}(z_4 - g(x,u,t)) \\ \dot{Z} = A_{21}Z + A_{22}u' \\ \dot{z}_4 = \beta_{04}u' \\ e = c_1^T X + c_2^T Z \\ u' = -\phi(e) \end{cases} \tag{23} $$

where $c_1 = [-1\ 0\ 0]^T$ and $c_2 = [1\ 0\ 0]^T \in R^n$.

Let $Y = A_{11}X + A_{13}Z_4$, then

$$ \begin{cases} \dot{Y} = A_{11}Y + A_{11}A_{12}Z + A_{13}\beta_{04}u' - A_{11}A_{13}g(x,u,t) \\ \dot{Z} = A_{21}Z + A_{22}u' \\ e = c_1^T A_{11}^{-1} Y + c_2^T Z - c_1^T A_{11}^{-1} A_{13} z_4 \\ u' = -\phi(e) \end{cases} \tag{24} $$

Rewrite (24) as

$$ \begin{cases} \dot{\tilde{x}} = A\tilde{x} + bu' + E(x,u) \\ \dot{\xi} = u' \\ e = c^T \tilde{x} + \rho\xi \\ u' = -\phi(e) \end{cases} \tag{25} $$

where

$$ \tilde{x} = [Y\ Z]^T, \quad E(x,u) = [-A_{11}A_{13}g(x,u,t)\ 0]^T, $$

$$ A = \begin{bmatrix} A_{11} & A_{11}A_{12} \\ 0 & A_{21} \end{bmatrix}, \quad b = \begin{bmatrix} A_{13}\beta_{04} \\ A_{22} \end{bmatrix}, \quad c^T = \begin{bmatrix} c_1^T A_{11}^{-1} & c_2^T \end{bmatrix} $$

and $\rho = -c_1^T A_{11}^{-1} A_{13}\beta_{04} = -\frac{\beta_{04}}{a_3}$.

System (25) can be expressed as the block diagram shown in Figure 3.

Ignoring the disturbance term $E(x,u)$, the linear transfer function of system (25) is as follows:

$$ G(s) = c^T (sI - A)^{-1} b + \rho/s \tag{26} $$

Definition 1 [40]: For the time-invariant nonlinear function denoted $\phi(e) \in F(0,k)$, if $\phi(e) = 0$, then $0 < \phi(e)e \le \delta^{\alpha-1}e^2, \forall e \neq 0$.

Definition 2 [41]: System (25) is said to be absolutely stable: if $\phi(e) \in F(0,k)$, the zero solutions of the system are globally consistently asymptotically stable; system (25) is said to be absolutely stable with a finite domain: if $\phi(e) \in F(0,k)$, the zero solutions of the system are consistently locally asymptotically stable.

2) STABILITY ANALYSIS

Lemma (Popov Criterion [41]): Assume that system (25) conforms to the following hypothesis.

(1) The matrix A is a Hurwitz matrix. The pair (A, b) is controllable, and the pair (A, c^T) is observable;

(2) $\rho > 0$ and $\phi(e) \in F(0,k)$;

(3) There exists a scalar $r' > 0$ such that the following inequality holds

$$ G_k(j\omega) = \frac{1}{k} + Re\left[(1 + j\omega r')G(j\omega)\right] > 0, \quad \forall\omega \in R \tag{27} $$

where $G_k(j\omega)$ is called the Popov function. The maximal k is called the Popov sector of system (25).

(4) Given a symmetric positive definite matrix W, there exists a scalar $\varepsilon > 0$, $\eta \ge 0$, a vector q, symmetric positive definite matrices P and W_0, and a scalar $\delta' > 0$ satisfying

$$ PA + A^T P = -qq^T - \varepsilon W \tag{28} $$

$$ Pb - \varsigma = \sqrt{\eta} q \tag{29} $$

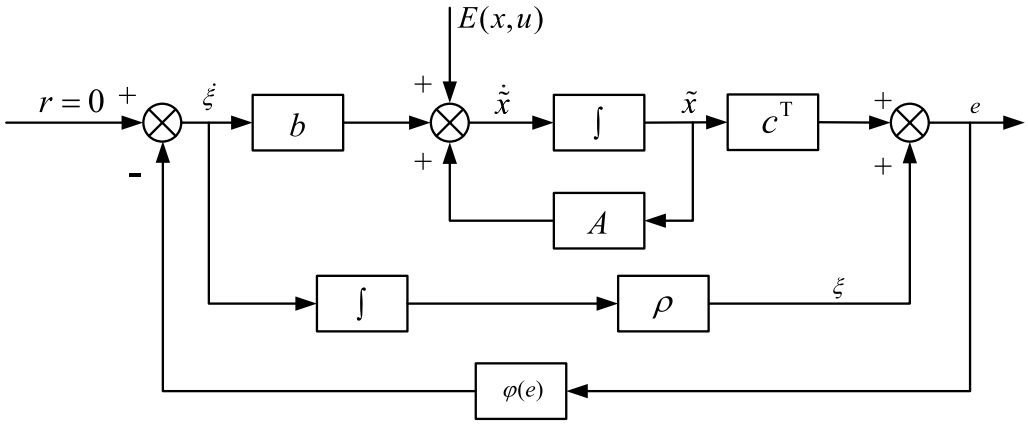

FIGURE 3. Block diagram of system (25).

$$\varepsilon W = \varepsilon W_0 + \delta' I \tag{30}$$

(5) The disturbance term $E(x, u)$ satisfies

$$\|E(x,u)\|_2 \le \beta \|\tilde{x}\|_2 \le \frac{\delta'}{2\|P\|_{i2} + r'k\|c\|_2^2} \|\tilde{x}\|_2 \tag{31}$$

where P_{i2} denotes the spectral norm of the matrix P, that is, $[\lambda_{\max}(P * P)]^{1/2}$. $\|\cdot\|_2$ represents the 2-norm and β is a positive real number.

Based on **Definition 2**, system (25) is uniformly and asymptotically stable under these assumptions.

Theorem: Under the action of controller (20), system (25) will be Popov-Lyapunov stable.

Proof: Construct a positive definite Lyapunov function, and then

$$V(\tilde{x}, e) = \tilde{x}^T P \tilde{x} + \alpha'(e - c^T\tilde{x})^2 + r' \int_0^e \phi(e)de \tag{32}$$

where P is a positive definite matrix; $\alpha', r' > 0$.

Suppose that for some $\theta > 0$, the set

$$\Omega_c = \left\{\tilde{x} \in R^{2n} | V(\tilde{x}) \le \theta\right\} \tag{33}$$

Formula (25) is substituted into Formula (32) to obtain

$$\begin{aligned}
&\dot{V}(\tilde{x}, e) \\
&= \left(\tilde{x}^T(PA + A^TP)\tilde{x}\right. \\
&\quad \left. +2((Pb)^T\tilde{x}u' + \tilde{x}^TPE(x,u))\right) + 2\alpha'(e - c^T\tilde{x})\rho u' \\
&\quad +r'\phi(e)\left(c^TA\tilde{x} - c^Tb\phi(e) + c^TE(x,u) - \rho\phi(e)\right) \\
&= \tilde{x}^T(PA + A^TP)\tilde{x} - 2\left(Pb - \alpha'\rho c - \frac{1}{2}r'A^Tc\right)^T \tilde{x}\phi(e) \\
&\quad +r'c^TE(x,u)\phi(e) - \left(\frac{2\alpha'\rho}{k} + r'\rho + r'c^Tb\right)\phi^2(e) \\
&\quad -2\alpha'\rho\phi(e)\left(e - \frac{1}{k}\phi(e)\right) + 2\tilde{x}^TPE(x,u)
\end{aligned} \tag{34}$$

Let

$$\begin{cases} \eta = \dfrac{2\alpha'\rho}{k} + r'\rho + r'c^Tb \\ \varsigma = \alpha'\rho c + \dfrac{1}{2}r'A^Tc \end{cases} \tag{35}$$

Then,

$$\begin{aligned}
\dot{V}(\tilde{x}, e) &= \tilde{x}^T(PA + A^TP)\tilde{x} - 2(Pb - \varsigma)^T\tilde{x}\phi(e) \\
&\quad +r'c^TE(x,u)\phi(e) - \eta\phi^2(e) \\
&\quad -2\alpha'\rho\phi(e)\left(e - \frac{1}{k}\phi(e)\right) + 2\tilde{x}^TPE(x,u)
\end{aligned} \tag{36}$$

Ultimately, $2\alpha'\rho\phi(e)\left(e - \frac{1}{k}\phi(e)\right) \ge 0$,

Let

$$\begin{aligned}
\dot{V}'(\tilde{x}, e) &= \tilde{x}^T(PA + A^TP)\tilde{x} - 2(Pb - \varsigma)^T\tilde{x}\phi(e) \\
&\quad -\eta\phi^2(e) + 2\tilde{x}^TPE(x,u) + r'c^TE(x,u)\phi(e)
\end{aligned} \tag{37}$$

Then,

$$\dot{V}(\tilde{x}, e) \le \dot{V}'(\tilde{x}, e) \tag{38}$$

Only if $\dot{V}'(\tilde{x}, e)$ is a negative definite function is $\dot{V}(\tilde{x}, e)$ a negative definite function. According to **Definition 1**,

$$0 < \phi(e) \le \delta^{\alpha-1}e, \quad \forall e > 0 \tag{39}$$

Then,

$$\|\phi(e)\|_2 \le \delta^{\alpha-1}\|e\|_2 \le k\left\|c^T\right\|_2 \|\tilde{x}\|_2 \tag{40}$$

Substitute Equation (40) into Equation (37) to obtain

$$\begin{aligned}
\dot{V}'(\tilde{x}, e) &\le \tilde{x}^T(PA + A^TP)\tilde{x} - 2(Pb - \varsigma)^T\tilde{x}\phi(e) \\
&\quad -\eta\phi^2(e) + 2\|\tilde{x}\|_2\|P\|_{i2}\|E(x,u)\|_2 \\
&\quad +r'k\|c\|_2^2\|\tilde{x}\|_2\|E(x,u)\|_2
\end{aligned} \tag{41}$$

Under **Lemma (5)**

$$\begin{cases} \|E(x,u)\|_2 \le \beta\|\tilde{x}\|_2 \\ 2\beta\|P\|_{i2} + r'k\beta\|c\|_2^2 \le \delta' \end{cases} \tag{42}$$

Substituting Equation (42) into Equation (41), we can obtain

$$\begin{aligned}&\dot{V}'(\tilde{x}, e)\\&\leq \tilde{x}^T(PA + A^TP)\tilde{x} - 2(Pb - \varsigma)^T\tilde{x}\phi(e)\\&\quad -\eta\phi^2(e) + \tilde{x}^T(2\beta\|P\|_{i2} + r'k\beta\|c\|_2^2)\tilde{x}\\&\leq \tilde{x}^T(PA + A^TP + \delta' I)\tilde{x} - 2(Pb - \varsigma)^T\tilde{x}\phi(e) - \eta\phi^2(e)\end{aligned} \tag{43}$$

According to **Lemma (4)**

$$\begin{aligned}\dot{V}'(\tilde{x}, e) &\leq \tilde{x}^T(-qq^T - \varepsilon W + \delta' I)\tilde{x}\\&\quad -2(Pb - \varsigma)^T\tilde{x}\phi(e) - \eta\phi^2(e)\\&\leq -\tilde{x}^T(\varepsilon W - \delta' I)\tilde{x} - \tilde{x}^T qq^T\tilde{x}\\&\quad -2(\sqrt{\eta}q)^T\tilde{x}\phi(e) - \eta\phi^2(e)\\&= -\tilde{x}^T(\varepsilon W - \delta' I)\tilde{x} - (\tilde{x}^T q + \sqrt{\eta}\phi(e))^2\end{aligned} \tag{44}$$

Substitute Equation (30) into (44), and then

$$\dot{V}'(\tilde{x}, e) \leq -\tilde{x}^T W_0\tilde{x} - (\tilde{x}^T q + \sqrt{\eta}\phi(e))^2 < 0 \tag{45}$$

Therefore, by combining Equation (38) with Equation (45), we can know that

$$\dot{V}(\tilde{x}, e) \leq \dot{V}'(\tilde{x}, e) < 0 \tag{46}$$

The proof is completed.

Thus, system (25) should be Popov-Lyapunov stable.

IV. NUMERICAL EXPERIMENTS

The improved ADRC is compared with the traditional ADRC and PID control strategy to evaluate its performance accurately. Table 2 shows the traditional ADRC parameters, and Table 3 shows the parameters of the improved ADRC. Under the condition of a mechanical time delay, the hydraulic turbine regulation system is verified via numerical simulation.

A. FO-NADRC AND THE EXISTING NADRC

The ESO is the key component for ensuring NADRC performance. The output error signal of the ESO directly influences the feedback loop of the controller to make an accurate response to the state variable of the HTRS. Therefore, when the HTRS considers the mechanical delay of the hydraulic servo device, the error signal can accurately forecast the NADRC control effect of the system state variables. The tracking effect of the improved ESO on the state variables is observed and compared with the classical ADRC under the mechanical delay, which is $\tau = 0.05$ s, 0.08 s, 0.10 s and 0.15 s. The time domain analysis of the error signals is shown in Figure 4 and Figure 5.

Figure 4 is the time-domain diagram of the error signal between the observed variables of the ESO and the state variables of the HTRS. Table 4 shows the performance indexes of the error signals between the system state and the observed state. First, Figure 4 shows that the error signal can finally reach a stable state, and that the ESO can effectively track and compensate the original signal. Second, from Figure 4(a) to Figure 4(d), the error signal has a slight chattering phenomenon after reaching stability under the action of traditional NADRC. The designed FO-NADRC is always maintained in a stable state. Under the control of NADRC, the stabilization time of the error signal x_1 in Figure 4(a), 4(b), 4(c) and 4(d) is 10.22 s, 12.57 s, 13.28 s, and 15.74 s, respectively. The stabilization time of the improved FO-NADRC is shortened by 4.657 s, 6.251 s, 6.522 s, and 8.373 s, respectively, compared to the traditional ADRC. The simulation results show that the chattering can be eliminated using the function $g(x, \sigma)$ instead of the function $f(x, \alpha, \delta)$. Moreover, the improved ESO enhances the observation performance and improves the performance of robust control of the control system. Figure 5 is the time-domain diagram of the error between the differential signal of the ESO observation variable and the differential signal of the HTRS state variable. The comparison between NADRC and FO-NADRC shows that the overshoot of error signal is substantially decreased under the control of FO-NADRC.

To sum up, the state variable of the HTRS finally reaches a stable state, which further verifies the effectiveness of the proposed controller. In addition, the obvious advantages of FO-NADRC in nonlinear systems are apparent by observing the change in the error signal. The proposed nonlinear function can effectively weaken the chattering of the stable system, which shows that it is superior to the traditional nonlinear function. Compared with the classical ADRC, the

TABLE 2. Parameters of the traditional NADRC.

Symbol	value	Symbol	value
r	20	β_{01}	25
h	0.01	β_{02}	250
α_1	0.75	β_{03}	2500
α_2	0.5	β_{04}	800
α_3	0.25	K_p	3.68
α_4	0.125	K_d	0.23
δ	0.01	b_0	0.56

TABLE 3. Parameters of the FO-NADRC.

Symbol	value	Symbol	value
r	10	β'_{03}	1372
h	0.01	β'_{04}	996
σ_1	1.25	K'_p	0.74
σ_2	0.75	K'_i	4.96
σ_3	0.50	K'_d	3.26
σ_4	0.125	λ	0.64
δ	0.01	γ	1.53
β'_{01}	28	b'_0	0.56
β'_{02}	284		

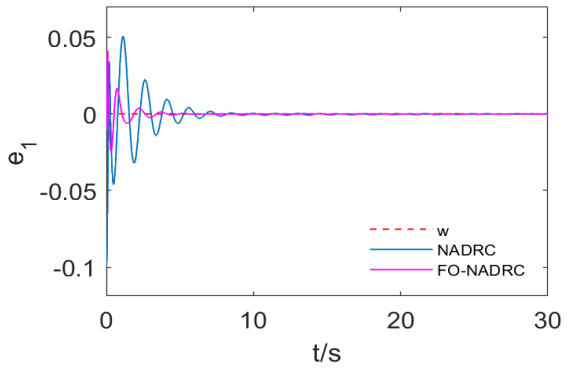

(a) $\tau = 0.05\ s$

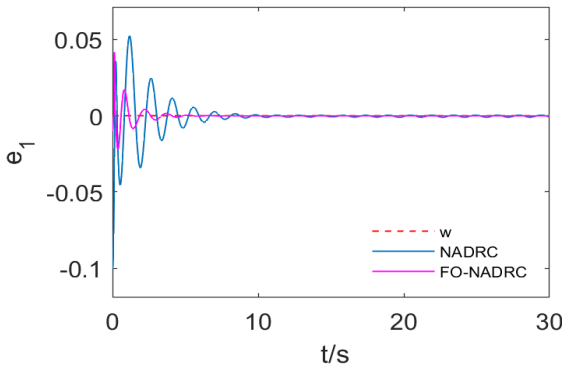

(b) $\tau = 0.08\ s$

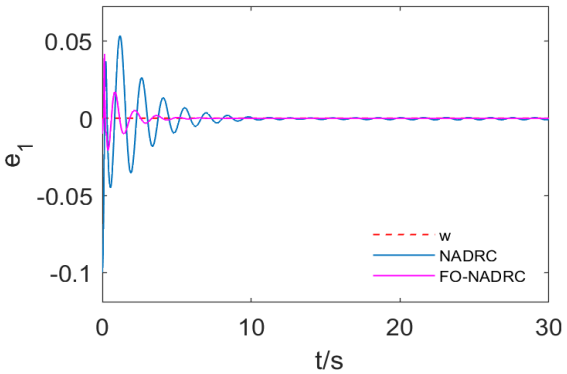

(c) $\tau = 0.1\ s$

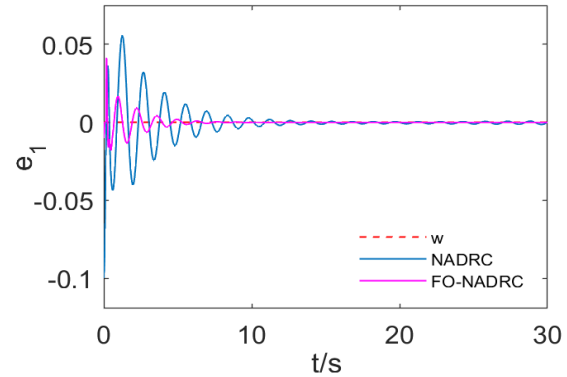

(d) $\tau = 0.15\ s$

FIGURE 4. Estimation error of the generator speed deviation x_1 for HTRS (3) under different time delays.

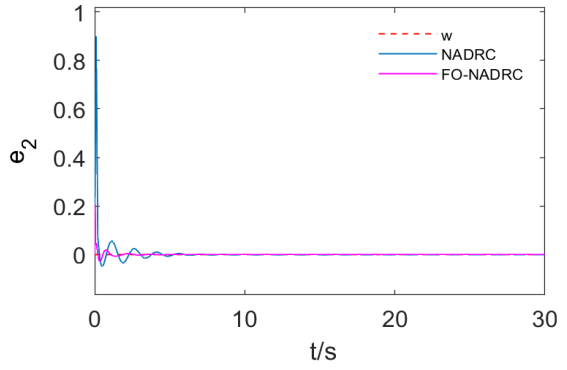

(a) $\tau = 0.05\ s$

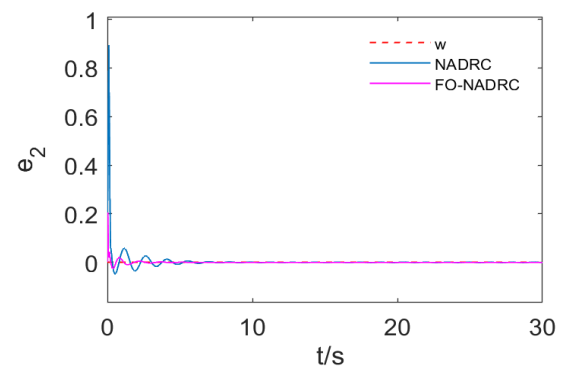

(b) $\tau = 0.08\ s$

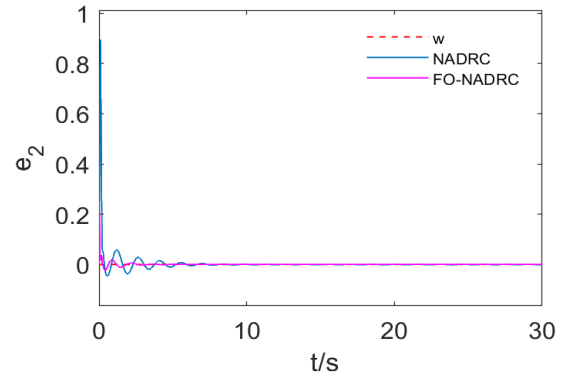

(c) $\tau = 0.1\ s$

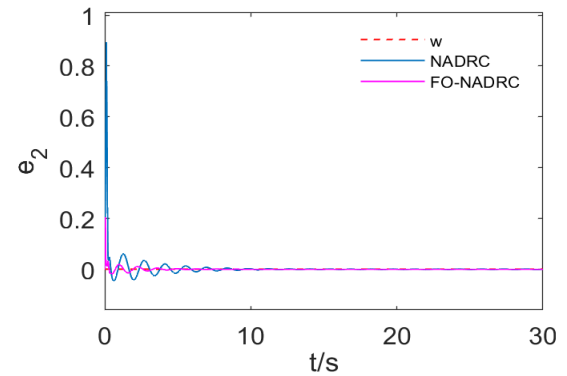

(d) $\tau = 0.15\ s$

FIGURE 5. Estimation error of the generator speed deviation x_2 for HTRS (3) under different time delays.

control effect of FO-NADRC is better than that of the classical NADRC under the mechanical delay that is considered.

B. FO-NADRC AND THE TRADITIONAL PID

The working condition of the turbine often changes in operation. When the unit load changes, the turbine flow must be changed to ensure the turbine power and load balance. Therefore, the movable guide vane plays a key role in regulating the unit capacity and frequency. Because of the mechanical inertia of the hydraulic amplifier, when the relay works, there will be a certain degree of time delay in the process of adjusting the opening of the movable guide vane. In this experiment, the influence of a mechanical delay term on the turbine speed is investigated.

To compare the control performances, the designed FO-NADRC method and PID control are adopted for $\tau = 0.05$ s, 0.08 s, 0.10 s, 0.15 s. The simulation results are shown in Figure 6. Table 5 shows the performance indexes of the HTRS transition process under different time delay characteristics.

The comparison in Figure 6 shows that NADRC can stabilize the state variables of the system. Second, the PID control effect of the HTRS gradually worsens with the increase in the time delay. The time delay has a deep influence on the generator speed deviation signal according to an analysis of the control performance. Because the mechanical delay is treated as an internal disturbance of the system, the controller is used to estimate the compensation disturbance to make the system return to a stable state. That is, when the hydro-generator set is disturbed, the generator speed will fluctuate slightly around the rated speed. From Figure 6(a) to 6(d), the generator needs 5.713 s, 6.391 s, 6.832 s, and 8.744 s to reach the rated speed, respectively. When $\tau > 0.1$ s, more than 30 s is required for the generator to reach a steady state under the control of PID. Therefore, compared with PID, FO-NADRC has the advantages of a short control time, small overshoot, and no buffeting after stabilization. The simulation results show that the designed FO-NADRC has good robustness, low overshoot, and fast recovery.

To sum up, the designed FO-NADRC has a smaller fluctuation and stronger anti-interference capability than the PID controller when the HTRS is disturbed. In addition, comparing the time delays with the attenuated oscillation period indicates that the time delays may lead to an increase in the attenuated oscillation period of the system signal. The proposed FO-NADRC effectively shortens the attenuation period of the speed deviation signal and makes the generator speed reach the stable speed quickly. Therefore, the FO-NADRC has the desired control performance under different time delays, which verifies the effectiveness of the proposed NADRC method.

C. LOAD FLUCTUATION CONDITION

As an important index for measuring the power quality, the operation frequency of the hydropower station has a

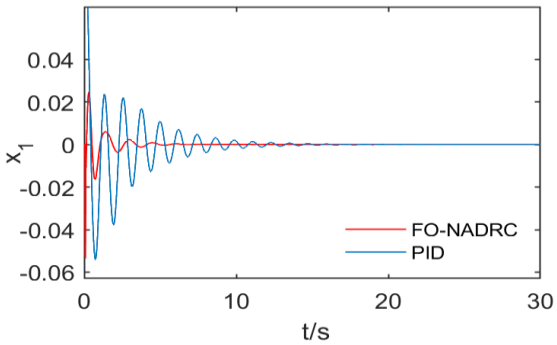

(a) $\tau = 0.05\ s$

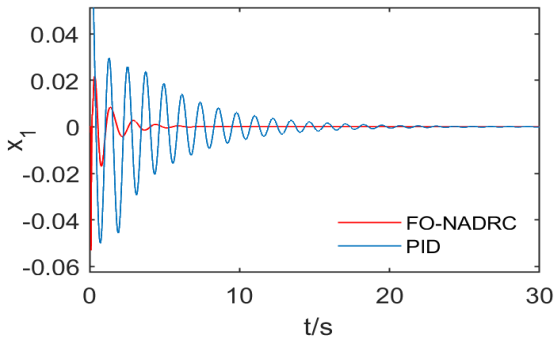

(b) $\tau = 0.08\ s$

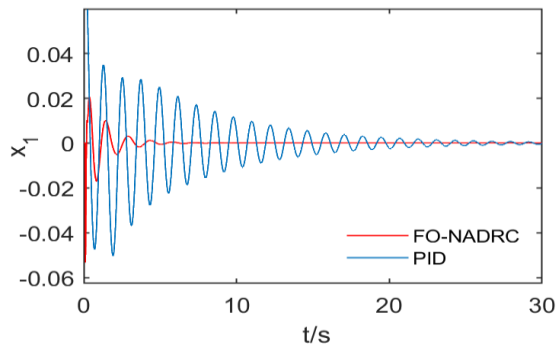

(c) $\tau = 0.1\ s$

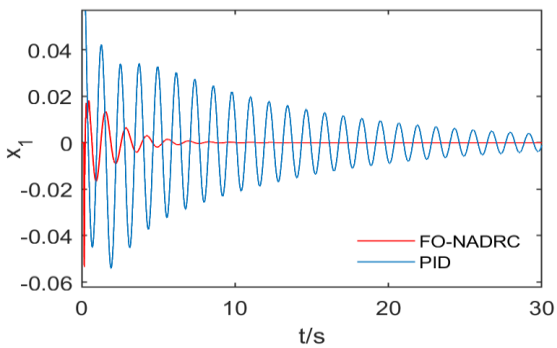

(d) $\tau = 0.15\ s$

FIGURE 6. NADRC and FO-NADRC for HTRS (3) under different time delays.

TABLE 4. Performance index of the error signal.

Estimated error	Conditions	NADRC		FO-NADRC	
	Time delays (s)	Wave peak	Transition time (s)	Wave peak	Transition time (s)
e_1	$\tau = 0.05$	0.098	10.22	0.0414	5.541
	$\tau = 0.08$	0.1	12.57	0.0416	6.319
	$\tau = 0.10$	0.1	15.74	0.0412	6.758
	$\tau = 0.15$	0.1	21.54	0.0413	7.367
e_2	$\tau = 0.05$	0.8979	10.11	0.2051	5.563
	$\tau = 0.08$	0.8934	12.57	0.2051	6.319
	$\tau = 0.10$	0.8945	15.32	0.2049	6.758
	$\tau = 0.15$	0.8945	18.01	0.2051	7.367

TABLE 5. Transition process performance indicators.

Conditions	PID		FO-NADRC	
Time delays (s)	Oscillation frequency	transition time (s)	Oscillation frequency	transition time (s)
$\tau = 0.05$	7	15.650	4	5.713
$\tau = 0.08$	12	>20	5	6.391
$\tau = 0.10$	>12	>20	5	6.832
$\tau = 0.15$	>12	>30	6	8.744

TABLE 6. Transition process performance indicators.

Conditions		NADRC		FO-NADRC	
Time (s)	Load fluctuation	Wave peak	transition time (s)	Wave peak	transition time (s)
t=0	5%	0.0551	10.21	0.0408	5.77
t=0	8%	0.0578	10.28	0.0403	5.84
t=15	5%	0.0061	5.84	0.0071	5.32
t=15	8%	0.0105	5.89	0.0102	5.40

high requirement. The frequency of the hydropower station is associated with the rotating speed of the hydroelectric generating set. Therefore, it is very important to adjust the generator speed to make it stable. The power system frequency range is ±0.2 Hz in China. In special cases, the frequency fluctuation range can reach ±1.0 Hz. During the operation of the hydropower station, the load of the generator often changes. In the transition process, the generator speed fluctuates and affects the stability of the system operation. In this experiment, 5% and 8% load fluctuations of the rated load are used as step signals to stimulate the generator set at 0 s and 15 s, respectively. The simulation results are shown in Figure 7.

Figure 7 shows that the relative deviation of the generator speed also has a corresponding fluctuation change when the speed of the hydro-generator is affected by the load fluctuation. Compared with NADRC, the generator speed can be quickly restored to the rated speed under the control of the FO-NADRC. By comparing Figure 7(a) with 7(c) and Figure 7(b) with 7(d), at 0 s and 15 s, the relative deviation of the generator speed has the step response of 5% and 8%, respectively. The generator speed can be quickly restored to the rated speed under the control of the improved FO-NADRC. By comparing Figures 7(a) and 7(b), under the control of NADRC, the generator speed reaches a stable state at 10.21 s and 10.28 s, respectively. Compared with NADRC, the response time of the improved FO-NADRC is reduced by 4.443 s and 4.442 s, and the overshoot decreases by 1.43% and 1.75%, respectively. When the hydroelectric generating set is subjected to load fluctuation, the comparison results show that the FO-NADRC has a stronger anti-fluctuation ability and faster recovery speed than the traditional ADRC.

Comparing Figure 7(c) and Figure 7(d) shows that more time is required for the generator speed to return to the specified speed with an increase in load fluctuation. When the load fluctuates by 5% at 15 s, the generator speed is stable within 5.32 s under the action of FO-NADRC. When the load fluctuates by 8% at 15 s, the generator speed reaches the specified speed at 5.4 s. With the increase in load fluctuation, more time is required for the generator speed to reach stability

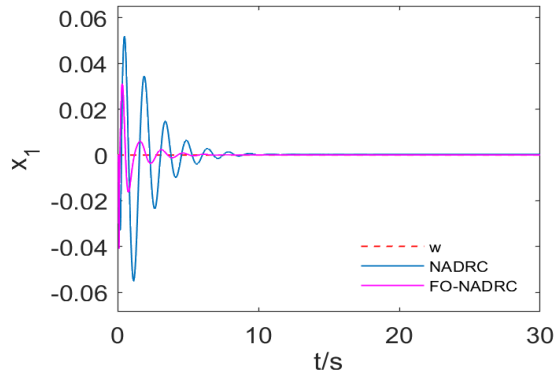

(a) $t = 0\ s,\ m_{g0} = 5\%$

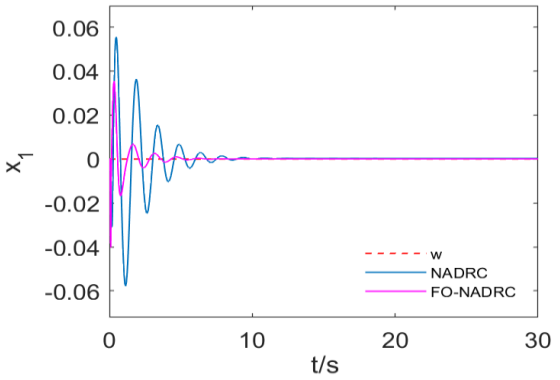

(b) $t = 0\ s,\ m_{g0} = 8\%$

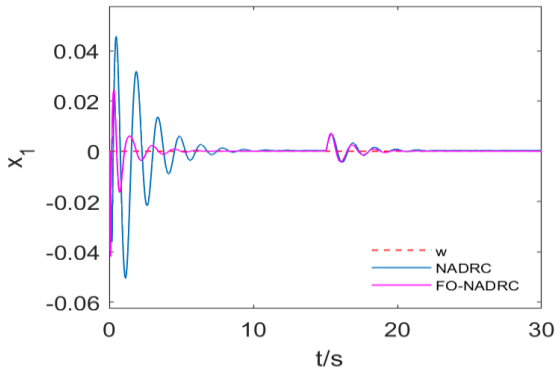

(c) $t = 15\ s,\ m_{g0} = 5\%$

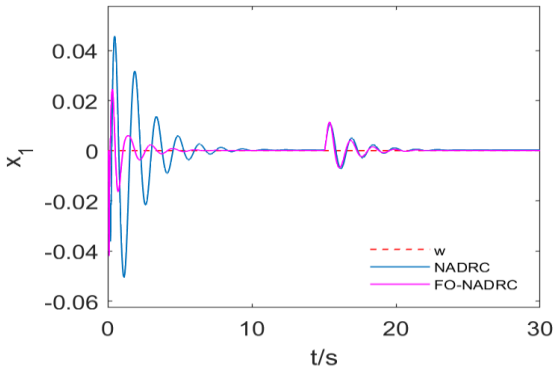

(d) $t = 15\ s,\ m_{g0} = 8\%$

FIGURE 7. NADRC and FO-NADRC for HTRS (3) under different load fluctuations at different times.

under the action of the controller. In conclusion, the proposed FO-NADRC has a better control effect on uncertain load fluctuation, which indicates the robustness of the proposed scheme.

D. PARAMETER SENSITIVITY ANALYSIS

1) INERTIA TIME CONSTANTS T_{ab}

T_{ab} represents the comprehensive index of inertial characteristics of the generator set. Physically, T_{ab} is the time required for the unit to accelerate from zero to the rated speed under the action of the rated torque M_r. T_{ab} is conducive to the stability of the regulation system; the greater the moment of inertia of the turbine is, the greater the value of T_{ab} will be.

The experimental results are shown in Figure 8. The inertial time constant of the unit is set as 15.0 s, 17.0 s, 22.0 s and 25.0 s in Figure 8(a), 8(b), 8(c) and 8(d), respectively. First, with the decrease in T_{ab}, the time for the generator to reach a stable speed decreases, and the overshoot increases. However, when T_{ab} is too small, the number of fluctuations increases, and the amplitude of the reversal process also increases. Second, the overall inertia of the HTRS increases when T_{ab} is too large. Although the amplitude of the system frequency fluctuation can be reduced, it slows down the dynamic process of the regulating system. Therefore, the choice of T_{ab} requires comprehensive consideration.

From Figure 8(a) to 8(d), as the delay time of relay increases, the time for the HTRS to reach stability increases, and the period of damped oscillation also increases under different T_{ab} conditions. Finally, the generator speed reaches a steady state under the action of the controller. In conclusion, it is suggested that the optimal selection range of T_{ab} is [17.0, 22.0].

2) COMPENSATION FACTOR b_0

In the disturbance compensation device (DCD), the selection of the correction coefficient b_0 has a great influence on the design of the controller. b_0 is primarily used to compensate and correct the error signal between the system state variable and the observation quantity of the observer. Therefore, the correction coefficient b_0 must be carefully adjusted to ensure the stability of the closed-loop system when designing the ADRC. In the simulation experiment, we set the correction coefficient as $b_0 = 1.0, 1.5, 2.0$, and 2.5. The experiment tests the control performance of the HTRS under different b_0. Figure 9 shows the simulation results.

First, with the increase in the time delay, Figure 9 shows that the control effect of the controller worsens or even fails when $b_0 = 1.0$. Second, with the increase in b_0, the time for the deviation signal of the generator speed to reach stability increases, and the overshoot decreases. Although the amplitude of the attenuation oscillation of the HTRS decreases, the time required for the generator speed to reach the rated speed increases when $b_0 = 2.5$. It can be speculated that the compensation effect of the correction coefficient b_0 on the feedback loop weakens when b_0 increases to a certain

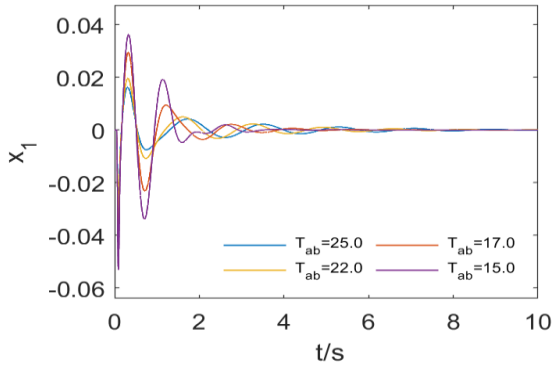

(a) $\tau = 0.05\ s$

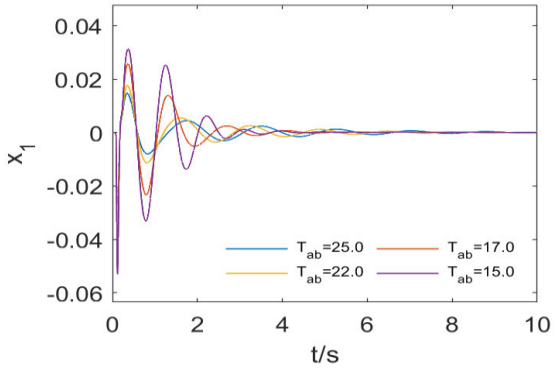

(b) $\tau = 0.08\ s$

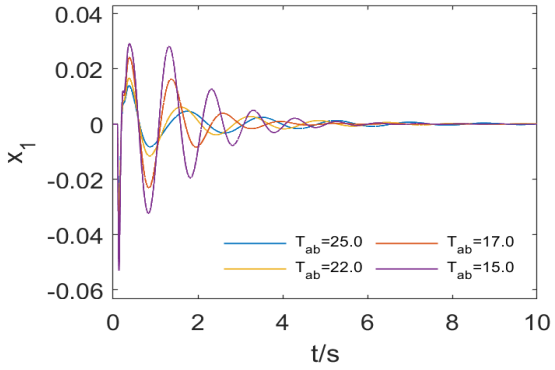

(c) $\tau = 0.10\ s$

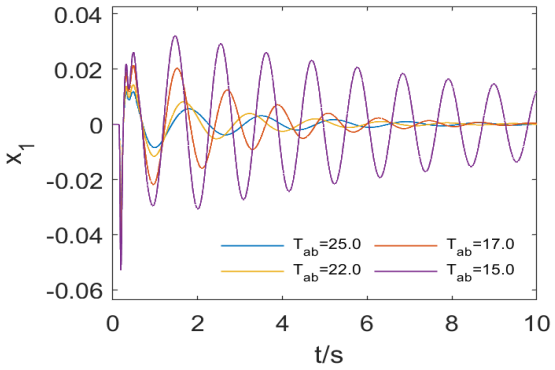

(d) $\tau = 0.15\ s$

FIGURE 8. FO-NADRC control for HTRS (3) with different time delays under different T_{ab}.

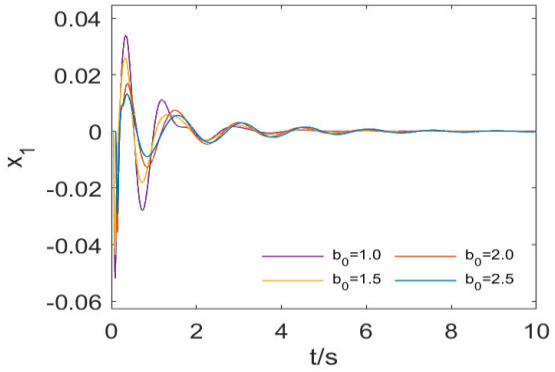

(a) $\tau = 0.05\ s$

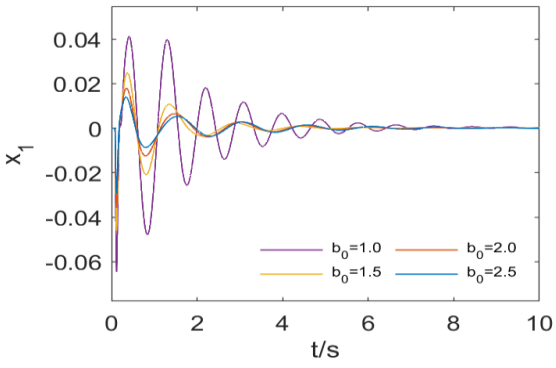

(b) $\tau = 0.08\ s$

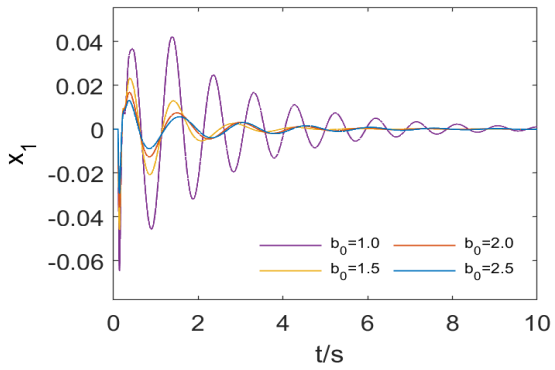

(c) $\tau = 0.10\ s$

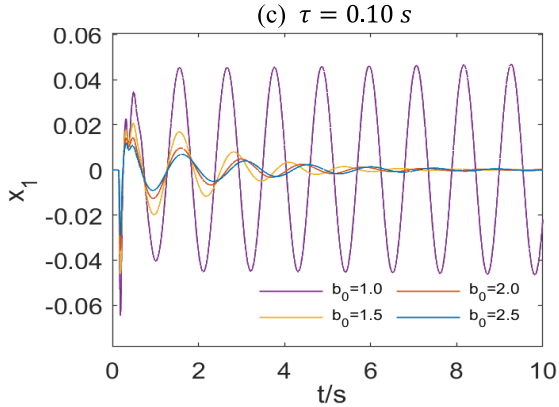

(d) $\tau = 0.15\ s$

FIGURE 9. FO-NADRC control for HTRS (3) with different time delays under different compensation factors.

value. Additionally, the damping oscillation period of the system will be longer. Therefore, the correction coefficient b_0 could not be infinite. To sum up, an oversized or undersized correction coefficient b_0 worsens the control effect of the controller. This experiment simulation suggests that the optimal selection range of b_0 is [1.5, 2.0].

V. CONCLUSION

In this study, a nonlinear fractional active disturbance rejection control is proposed to stabilize a nonlinear hydraulic turbine regulating system with a mechanical delay. First, the hydraulic turbine regulating system with a mechanical delay is converted into a matched active disturbance rejection control model using the coordinate transformation method. Second, a new nonlinear extended state observer is designed based on the basic form of the classical observer. Third, based on the classical state error feedback law and introducing two adjustable parameters, a new adjustable fractional-order feedback control is proposed. Fourth, a novel nonlinear fractional active disturbance rejection control with a time delay nonlinear hydraulic turbine regulating system is designed. Finally, the nonlinear hydraulic turbine regulating system with a time delay is numerically tested considering model matching and load disturbance. Although the control effect of the hydraulic turbine regulation system worsens with the increase in the mechanical delay of the hydraulic servo system, the improved fractional active disturbance rejection speed controller can accelerate the response speed of the system signal with a small overshoot. The speed can reach a stable value within 10 s under the action of the fractional active disturbance rejection speed controller. The fractional active disturbance rejection controller effectively eliminates the defects of system oscillation after stabilization. The proposed fractional-order active disturbance rejection speed controller has a strong anti-interference ability and can quickly compensate for disturbance signals. Numerical experiments verify the effectiveness and robustness of the proposed controller.

This study has shortcomings. In the actual operation process of a hydropower station, there is not only mechanical delay caused by the hydraulic servo system but also hydraulic delay caused by the water hammer effect of the pressure pipeline. Moreover, in the simulation experiment of the control system parameters, we find that the parameters have a great influence on the control effect of the controller. Therefore, parameter optimization remains a difficult problem in complex nonlinear control systems. Therefore, research on the control problem of the nonlinear hydraulic turbine regulating systems will remain the key work in the future.

CONFLICT OF INTERESTS

The authors declare that there is no conflict of interests regarding the publication of this article.

REFERENCES

[1] Y.-C. Tsai, Y.-K. Chan, F.-K. Ko, and J.-T. Yang, "Integrated operation of renewable energy sources and water resources," *Energy Convers. Manage.*, vol. 160, pp. 439–454, Mar. 2018.

[2] D. Zhang, J. Wang, Y. Lin, Y. Si, C. Huang, J. Yang, B. Huang, and W. Li, "Present situation and future prospect of renewable energy in China," *Renew. Sustain. Energy Rev.*, vol. 76, pp. 865–871, Sep. 2017.

[3] C. Penghao, L. Pingkuo, and P. Hua, "Prospects of hydropower industry in the Yangtze river basin: China's green energy choice," *Renew. Energy*, vol. 131, pp. 1168–1185, Feb. 2019.

[4] Y. Sun, "The achievement, significance and future prospect of China's renewable energy initiative," *Int. J. Energy Res.*, vol. 44, no. 15, pp. 12209–12244, Dec. 2020.

[5] H. Zhang, D. Chen, C. Wu, and X. Wang, "Dynamics analysis of the fast-slow hydro-turbine governing system with different time-scale coupling," *Commun. Nonlinear Sci. Numer. Simul.*, vol. 54, pp. 136–147, Jan. 2018.

[6] W. M. Ahmad and A. M. Harb, "On nonlinear control design for autonomous chaotic systems of integer and fractional orders," *Chaos, Solitons Fractals*, vol. 18, no. 4, pp. 693–701, Nov. 2003.

[7] J. Song, L. Wang, G. Cai, and X. Qi, "Nonlinear fractional order proportion-integral-derivative active disturbance rejection control method design for hypersonic vehicle attitude control," *Acta Astronautica*, vol. 111, pp. 160–169, Jun. 2015.

[8] D. Baleanu, R. L. Magin, S. Bhalekar, and V. Daftardar-Gejji, "Chaos in the fractional order nonlinear bloch equation with delay," *Commun. Nonlinear Sci. Numer. Simul.*, vol. 25, nos. 1–3, pp. 41–49, Aug. 2015.

[9] C. Yin, S. M. Zhong, and W. F. Chen, "Design of sliding mode controller for a class of fractional-order chaotic systems," *Commun. Nonlinear Sci. Numer. Simul.*, vol. 17, no. 1, pp. 356–366, 2012.

[10] Z. Chen, X. Yuan, B. Ji, P. Wang, and H. Tian, "Design of a fractional order PID controller for hydraulic turbine regulating system using chaotic non-dominated sorting genetic algorithm II," *Energy Convers. Manage.*, vol. 84, pp. 390–404, Aug. 2014.

[11] W. Guo and J. Yang, "Hopf bifurcation control of hydro-turbine governing system with sloping ceiling tailrace tunnel using nonlinear state feedback," *Chaos, Solitons Fractals*, vol. 104, pp. 426–434, Nov. 2017.

[12] H. Zhang, D. Chen, B. Xu, C. Wu, and X. Wang, "The slow-fast dynamical behaviors of a hydro-turbine governing system under periodic excitations," *Nonlinear Dyn.*, vol. 87, no. 4, pp. 2519–2528, Mar. 2017.

[13] P. Chen, B. Wang, Y. Tian, and Y. Yang, "Finite-time stability of a time-delay fractional-order hydraulic turbine regulating system," *IEEE Access*, vol. 7, pp. 82613–82623, 2019.

[14] B. Xu, D. Chen, H. Zhang, F. Wang, X. Zhang, and Y. Wu, "Hamiltonian model and dynamic analyses for a hydro-turbine governing system with fractional item and time-lag," *Commun. Nonlinear Sci. Numer. Simul.*, vol. 47, pp. 35–47, Jun. 2017.

[15] Y. Yi, D. Chen, H. Li, C. Li, and J. Zhou, "Observer-based adaptive output feedback fault tolerant control for nonlinear hydro-turbine governing system with state delay," *Asian J. Control*, vol. 22, no. 1, pp. 192–203, Jan. 2020.

[16] H. Jin, J. Song, W. Lan, and Z. Gao, "On the characteristics of ADRC: A PID interpretation," *Sci. China Inf. Sci.*, vol. 63, no. 10, Oct. 2020, Art. no. 209201.

[17] H. Rezaee and F. Abdollahi, "Motion synchronization in unmanned aircrafts formation control with communication delays," *Commun. Nonlinear Sci. Numer. Simul.*, vol. 18, no. 3, pp. 744–756, Mar. 2013.

[18] Z. Wu, D. Li, and Y. Chen, "Active disturbance rejection control design based on probabilistic robustness for uncertain systems," *Ind. Eng. Chem. Res.*, vol. 59, no. 40, pp. 18070–18087, Oct. 2020.

[19] T. Q. Xie, Y. Li, Y. Q. Jiang, L. An, and H. W. Wu, "Backstepping active disturbance rejection control for trajectory tracking of underactuated autonomous underwater vehicles with position error constraint," *Int. J. Adv. Robot. Syst.*, vol. 17, no. 2, Mar. 2020, Art. no. 1729881420909633.

[20] Y. X. Su, C. H. Zheng, and B. Y. Duan, "Automatic disturbances rejection controller for precise motion control of permanent-magnet synchronous motors," *IEEE Trans. Ind. Electron.*, vol. 52, no. 3, pp. 814–823, Jun. 2005.

[21] F. Liu, Y. Li, Y. Cao, J. She, and M. Wu, "A two-layer active disturbance rejection controller design for load frequency control of interconnected power system," *IEEE Trans. Power Syst.*, vol. 31, no. 4, pp. 3320–3321, Jul. 2016.

[22] W. Deng, J. Yao, and D. Ma, "Time-varying input delay compensation for nonlinear systems with additive disturbance: An output feedback approach," *Int. J. Robust Nonlinear Control*, vol. 28, no. 1, pp. 31–52, Jan. 2018.

[23] S. Zhao and Z. Gao, "Modified active disturbance rejection control for time-delay systems," *ISA Trans.*, vol. 53, no. 4, pp. 882–888, Jul. 2014.

[24] W. Deng, J. Yao, and D. Ma, "Adaptive control of input delayed uncertain nonlinear systems with time-varying output constraints," *IEEE Access*, vol. 5, pp. 15271–15282, 2017.
[25] Q. Liu, "Observer-predictor feedback for consensus of discrete-time multiagent systems with both state and input delays," *Int. J. Robust Nonlinear Control*, vol. 30, no. 10, pp. 4003–4021, Jul. 2020.
[26] W. Tan and C. Fu, "Linear active disturbance-rejection control: Analysis and tuning via IMC," *IEEE Trans. Ind. Electron.*, vol. 63, no. 4, pp. 2350–2359, Apr. 2016.
[27] S. Chen, W. Xue, S. Zhong, and Y. Huang, "On comparison of modified ADRCs for nonlinear uncertain systems with time delay," *Sci. China Inf. Sci.*, vol. 61, no. 7, p. 70223, Jul. 2018.
[28] M. Ran, Q. Wang, C. Dong, and L. Xie, "Active disturbance rejection control for uncertain time-delay nonlinear systems," *Automatica*, vol. 112, Feb. 2020, Art. no. 108692.
[29] Z.-L. Zhao and B.-Z. Guo, "A nonlinear extended state observer based on fractional power functions," *Automatica*, vol. 81, pp. 286–296, Jul. 2017.
[30] B.-Z. Guo, Z.-H. Wu, and H.-C. Zhou, "Active disturbance rejection control approach to output-feedback stabilization of a class of uncertain nonlinear systems subject to stochastic disturbance," *IEEE Trans. Autom. Control*, vol. 61, no. 6, pp. 1613–1618, Jun. 2016.
[31] J. Huang, P. Ma, G. Bao, F. Gao, and X. Shi, "Research on position servo system based on fractional-order extended state observer," *IEEE Access*, vol. 8, pp. 102748–102756, 2020.
[32] D. Ling and Y. Tao, "An analysis of the hopf bifurcation in a hydroturbine governing system with saturation," *IEEE Trans. Energy Convers.*, vol. 21, no. 2, pp. 512–515, Jun. 2006.
[33] F. Wang, D. Chen, B. Xu, and H. Zhang, "Nonlinear dynamics of a novel fractional-order francis hydro-turbine governing system with time delay," *Chaos, Solitons Fractals*, vol. 91, pp. 329–338, Oct. 2016.
[34] G. Liang, W. Li, and Z. Li, "Control of superheated steam temperature in large-capacity generation units based on active disturbance rejection method and distributed control system," *Control Eng. Pract.*, vol. 21, no. 3, pp. 268–285, Mar. 2013.
[35] J. Han, "From PID to active disturbance rejection control," *IEEE Trans. Ind. Electron.*, vol. 56, no. 3, pp. 900–906, Mar. 2009.
[36] X. Shao and H. Wang, "Active disturbance rejection based trajectory linearization control for hypersonic reentry vehicle with bounded uncertainties," *ISA Trans.*, vol. 54, pp. 27–38, Jan. 2015.
[37] J. Cortés-Romero, E. Delgado-Aguilera, and A. Jimenez-Triana, "Robust fractional active disturbance rejection control: A unified approach," *ISA Trans.*, vol. 107, pp. 63–77, Dec. 2020.
[38] J. R. Nayak, B. Shaw, and B. K. Sahu, "Implementation of hybrid SSA–SA based three-degree-of-freedom fractional-order PID controller for AGC of a two-area power system integrated with small hydro plants," *IET Gener., Transmiss. Distrib.*, vol. 14, no. 13, pp. 2430–2440, Jul. 2020.
[39] K. Erenturk, "Fractional order and active disturbance rejection control of nonlinear two-mass drive system," *IEEE Trans. Ind. Electron.*, vol. 60, no. 9, pp. 3806–3813, Sep. 2013.
[40] X. Qi, J. Li, Y. Xia, and Z. Gao, "On the robust stability of active disturbance rejection control for SISO systems," *Circuits, Syst., Signal Process.*, vol. 36, no. 1, pp. 65–81, Jan. 2017.
[41] J. Li, Y. Xia, X. Qi, and P. Zhao, "Robust absolute stability analysis for interval nonlinear active disturbance rejection based control system," *ISA Trans.*, vol. 69, pp. 122–130, Jul. 2017.

BO AI was born in Henan, China, in 1996. He received the B.E. degree in energy and power engineering from Northwest A&F University, where he is currently pursuing the graduate degree in water conservancy project. His research interest includes stability and active disturbance rejection control of hydropower systems.

TING LIU was born in Shaanxi, China. She is currently pursuing the degree majoring in electrical engineering and automation with Northwest A&F University. Her research interest includes software and hardware design of speed regulation system for hydropower station.

ZHE ZHANG received the B.E. degree in energy and power engineering from Northwest A&F University, where she is currently pursuing the graduate degree in water conservancy project. Her research interest includes stability and predictive functional control of hydropower systems.

BIN WANG (Member, IEEE) received the B.E. degree in electrical engineering from Xi'an Jiaotong University, Xi'an, China, in 2008, and the Ph.D. degree in agricultural soil and water engineering from Northwest A&F University, in 2017. He is currently an Associate Professor with the Department of Electrical Engineering, Northwest A&F University. His research interest includes modeling and coordinated control of water wind hybrid power generation systems.